Opto-Electronics Review

journal homepage: https://journals.pan.pl/opelre

Numerical analysis of tunable edge filters based on hyperbolic metamaterials constructed from indium tin oxide and silicon oxide layers

Karol Sielezin*, Michał Dudek, Urszula Chodorow, Janusz Parka

Institute of Applied Physics, Military University of Technology, ul. gen. Kaliskiego 2, 00-908 Warsaw, Poland

Article info

Article history:
Received 06 Jul. 2024
Received in revised form 24 Oct. 2024
Accepted 07 Nov. 2024
Available on-line 23 Dec. 2024

Keywords:
hyperbolic metamaterials (HMMs);
indium tin oxide (ITO);
transparent conductive oxides (TCOs);
transfer matrix method (TMM);
finite-difference time-domain (FDTD).

Abstract

This paper presents and discusses the results of numerical studies of multi-layered hyperbolic metamaterials (HMMs). Such structures are built of alternating thin layers of conductive (e.g., metal or alternative conductive material) and dielectric materials. The thicknesses of these layers are much smaller than the operating wavelength, usually of the order of a few or tens of nanometres. Indium tin oxide (ITO), which is an alternative conductive plasmonic material from the group of transparent conductive oxides (TCOs), was used in the conductive layers. Silica (SiO_2) was used as a material in the dielectric layers. As a result of a simulation-based optimization, the layer thicknesses of two components forming the structure were chosen to be 20 nm each. Four variants of multilayer structures with different numbers of elementary cells forming the structure, N, for $N = 5$, 10, 15, and 20, respectively, were investigated by both analytical methods using the transfer matrix method (TMM) and simulation methods using finite-difference time-domain (FDTD). The results confirmed the hyperbolic dispersion of effective electric permittivity and tunability of the structure in the near-infrared (NIR) range. Moreover, a complete agreement of the results confirmed the complementarity of the two methods – both analytical TMM and simulation FDTD. The proposed HMMs structures may have potential applications as tunable edge filters.

1. Introduction

Hyperbolic metamaterials (HMMs) are a fairly new class of anisotropic materials whose non-trivial electromagnetic properties result from the nanostructure and appropriately spatially located elementary cells called meta-atoms. An appropriately structured HMM acquires completely new and different properties from the constitutive materials from which the HMM structure was constructed. Hence, the term metamaterial, since 'meta' in Greek means 'beyond'. Thus, by analogy, given the morphology of materials made of atoms, metamaterials are nanostructures built of meta-atoms [1–3].

However, it should be noted that the optical properties of another class of engineering materials – photonic crystals – are also determined by their structure but there is a fundamental difference between these two classes of engineering materials. That difference is the length scales of their elementary cells. Although the period and unit cell size of photonic crystals are comparable to the wavelength of light, the size of a meta-atom is much smaller than the wavelength of light. Hence, metamaterials can be considered as optically active effective media, while photonic crystals cannot be considered as such [1].

Taking into account the properties of materials related to their interaction with electromagnetic waves, then, according to the considerations of Veselago [4], propagation of electromagnetic waves is only possible in materials with positive or negative values of both permittivity ε_r and permeability μ_r. In the case of classical materials referred to as positive media (also known as 'right-handed media'), the relationship $\varepsilon_r, \mu_r > 0$, occurs. In contrast, a characteristic feature of metamaterials are negative values of the permittivity ε_r (the relationship $\varepsilon_r < 0$

*Corresponding author at: karol.sielezin@wat.edu.pl

https://doi.org/10.24425/opelre.2024.152767
1896-3757/ Association of Polish Electric Engineers (SEP) and Polish Academic of Sciences (PAS). Published by PAS

occurs) and, consequently, negative values of the refractive index for these materials which belong to the group referred to as negative media (also called 'left-handed media') [1, 5, 6].

Originally, HMM structures were to be used to overcome the diffraction limit in optical imaging. However, as a result of further research, it turned out that HMMs have several new and unique properties, especially regarding their interaction with electromagnetic waves. The properties of HMMs and the phenomena occurring within them include super-resolution imaging [1, 2, 7–9], nanolithography [10], ability to enhance quantum-electrodynamic effects, e.g., Purcell effect [1, 2, 9–13], thermal superconductivity phenomena [1, 3, 9, 10, 14, 15], photonic bandgap engineering [16–18], possibility of active tunability of photonic devices [1, 2, 10], and development of technology that gives impression of invisibility [1, 2, 9, 10].

Thus, in line with what has already been written, metamaterials differ from classical materials primarily by different properties relating to interactions with electromagnetic waves. In the case of an isotropic material, the isofrequency surface is the sphere described by equation:

$$k_x^2 + k_y^2 + k_z^2 = \varepsilon_r \mu_r \left(\frac{\omega}{c}\right)^2, \tag{1}$$

where the wave vector $\vec{k}$ is described by the components: $\vec{k} = [k_x, k_y, k_z]$, ε_r and μ_r denote the relative permittivity and relative permeability of the medium, respectively, ω denotes the angular frequency of the electromagnetic wave propagating in the medium, and c is the velocity of the electromagnetic wave in a vacuum. For an anisotropic material, permittivity is described by the diagonal tensor:

$$\overline{\varepsilon} = \mathrm{diag}\left[\varepsilon_{xx}, \varepsilon_{yy}, \varepsilon_{zz}\right], \tag{2}$$

where all components have positive values, with $\varepsilon_{xx} = \varepsilon_{yy} = \varepsilon_{\parallel}$ and $\varepsilon_{zz} = \varepsilon_{\perp}$. In such case, the isofrequency surface is the ellipsoid described by [10]:

$$\frac{k_x^2 + k_y^2}{\varepsilon_{zz}} + \frac{k_Z^2}{\varepsilon_{xx}} = \left(\frac{\omega}{c}\right)^2. \tag{3}$$

When considering surfaces of constant frequencies in HMMs, two types are distinguished depending on whether only one of the components of the permittivity tensor takes a negative value (Type-I HMM), or if two of the components are negative (Type-II HMM). A distinction is made, respectively, between HMM Type I, in which: $\varepsilon_{xx}, \varepsilon_{yy} > 0$, $\varepsilon_{zz} < 0$,so $\varepsilon_{\parallel} > 0$, and $\varepsilon_{\perp} < 0$ and the isofrequency surface forms the two-shell hyperboloid, and HMM Type II in which: $\varepsilon_{xx}, \varepsilon_{yy} < 0$, $\varepsilon_{zz} > 0$, so $\varepsilon_{\parallel} < 0$ and $\varepsilon_{\perp} > 0$ for which the constant-frequency surface is a single-shell hyperboloid [1, 2, 9, 10, 19].

A frequently used approach to achieve hyperbolic dispersion of effective permittivity properties is constructing an HMM structure made of thin metal/dielectric layers (constituting an elementary cell). This approach is based on depositing very thin layers alternating between metal and dielectric, whereby, in order to achieve a homogeneous structure, the thickness of these layers must in practice be at least ten times smaller than the electromagnetic wavelength with which the HMM structure is to interact. The application of the effective medium theory (EMT) allows to represent the components of the dielectric tensor in the form of equations below [10]:

$$\varepsilon_{\parallel} = \rho\varepsilon_m + (1-\rho)\varepsilon_d \tag{4}$$

$$\varepsilon_{\perp} = \frac{\varepsilon_m \varepsilon_d}{\rho\varepsilon_d + (1-\rho)\varepsilon_m}, \tag{5}$$

where $\rho = \frac{d_m}{d_m + d_d}$ – the filing ratio of metal layer, ε_m – the relative permittivity of metal, ε_d – the relative permittivity of dielectric, d_m – the thickness of metal layer, d_d – the thickness of dielectric layer.

The EMT allows to explain that under the right conditions both types of structures (HMMs Type I and Type II) are able to achieve the required extreme anisotropy of permittivity. Moreover, it can be tuned in most of the wavelength ranges of interest – UV, VIS, NIR, and MIR – with the right choice of constitutive materials (metal and dielectric), as well as the right choice of geometrical parameters for the HMM structure, so that the appropriate resonance effect can occur [20–23].

One of the promising alternative conductive materials that can be used in HMM structures are transparent conductive oxides (TCOs), i.e., oxide semiconductors such as, e.g., indium oxide, zinc oxide, or cadmium oxide. Appropriate doping of these oxides affects their conductive properties which is why they are commonly used in display panels where they form electric contacts. One of the most popular materials in the TCO group is indium tin oxide (ITO). Its electric properties can be modified and tuned accordingly by doping with other oxides [24].

In several previous works in which the authors investigated other structures of HMMs, they equally demonstrated the possibility of using these structures as tunable filters [21, 23, 25]. Other publications have also described possible applications of HMM structures for the construction of tunable edge filters [26–28].

This paper presents the results of numerical simulations of multi-layered HMM structures using ITO as a conductive layer and SiO_2 as a dielectric layer. The designed HMM structures were investigated by both analytical methods using the transfer matrix method (TMM) and simulation methods using finite-difference time-domain (FDTD). Fabrication of the proposed microstructures is beyond the scope of the presented study.

2. Materials and methods

Four series of multi-layered HMM structures consisting of alternating layers of 20 nm ITO and 20 nm SiO_2 were investigated for different numbers of elemental cells: $N = 5$, 10, 15, and 20, respectively. A schematic image of the ITO/SiO_2 structure for $N = 5$ is shown in Fig. 1.

Simulations were carried out in the ANSYS/Lumerical software. Material data for SiO_2 thin films for the simulation process were taken from Palik [29]. In the case of ITO, the relevant permittivity data were obtained through measurements of thin films of ITO using spectroscopic ellipsometry [23]. The measured ITO films had a thickness

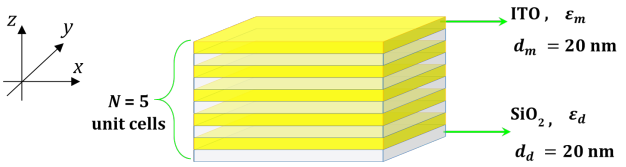

Fig. 1. Scheme of the investigated ITO/SiO_2 HMM multi-layered structure for $N = 5$.

of 20 ± 3 nm and surface resistivity of about 100 Ω/sq. All simulations were carried out in the range of 300–2500 nm. Characterisation of the properties such as effective permittivity, absorbance, transmittance, and reflectance for the investigated multi-layered HMMs structures was performed using an analytical procedure – TMM – and a simulation method requiring the definition of an appropriate model – FDTD.

3. Results and discussion

Figure 2 illustrates the results of simulations in the range of 0.3–2.5 μm for the real part (Re) and imaginary part (Im) of the components of the tensor of effective permittivity characterising the studied multi-layer HMM structure.

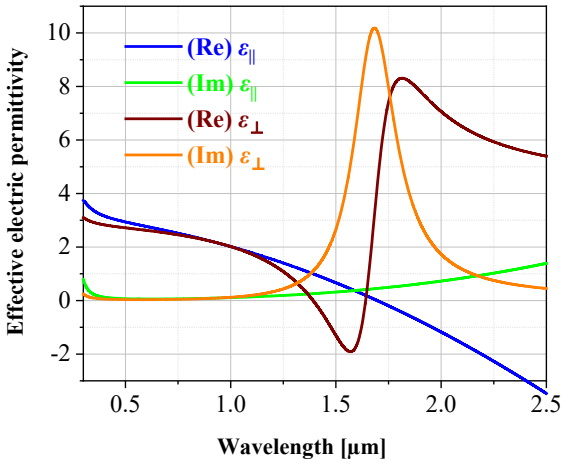

Fig. 2. Simulation results of the components of the effective permittivity tensor obtained for the multi-layer structure (20 nm ITO/20 nm SiO_2), real part (Re) and imaginary part (Im) of the components of the permittivity tensor $\varepsilon_{\parallel}$ and $\varepsilon_{\perp}$ for the studied multi-layer structure.

From the analysis of Fig. 2, it can be seen that the values of the Re of $\varepsilon_{\parallel}$ decrease monotonically over the entire range considered, with values above about 1700 nm becoming negative. The Im of $\varepsilon_{\parallel}$ takes on non-negative values over the entire range under consideration. The Re of $\varepsilon_{\perp}$ decreases in the range from 300 nm to about 1600 nm, after which it increases, reaching the maximum at about 1800 nm after which it decreases, taking on positive values. The Im of $\varepsilon_{\perp}$ increases in the range from 300 nm, taking its maximum at about 1700 nm after which it decreases in the further range, taking positive values. Thus, it can be concluded that in the range from about 1400 nm to about 1650 nm, the structure exhibits Type I hyperbolic dispersion [negative value of the component Re($\varepsilon_{\perp}$) in this range], while above 1700 nm it transitions to Type II hyperbolic dispersion [negative value of the Re($\varepsilon_{\parallel}$) component over the entire further examined range].

In order to characterise the transmission and reflection properties of the studied multi-layered structures, successive simulations of transmittance and reflectance spectra were carried out using TMM for different numbers of elementary cells building the structure – successively using 5, 10, 15, and 20 elementary cells in the structures ($N = 5$, 10, 15, 20). The results of these simulations are summarized in Fig. 3.

In the case of the studied HMM structures, an increase in the number of elementary cells in the structure results in steeper reflectance characteristics, increasing the chance of using such a structure as a tunable edge filter. At the same time, increasing the number of layers in the structure shifts the transition wavelength towards shorter wavelengths (blueshift) from about 2200 nm for $N = 5$ to about 1600 nm for $N = 20$, and also introduces higher absorbance in the transition region. One of the less evident but important features of this HMM structure is the fact that while the reflectance remains at the same level above the transition wavelength, the region below this wavelength is dominated by the interplay between the transmittance (influenced mostly by SiO_2 properties) and absorbance (influenced mostly by ITO properties). Therefore, with an increasing number of cells, the transmittance level decreases slowly but continuously which is an important factor for a proper filter design. The studied structure also shows the possibility of tunability in the NIR range with the change in the number of elementary cells.

In order to further verify the properties of the investigated multi-layered structures constructed from ITO/SiO_2 layers, spatial distributions of reflectance and transmittance as a function of incident angle were simulated using the FDTD method. Summarized results of these simulations are illustrated in the following Fig. 4 and Fig. 5.

Figure 4 illustrates the spatial distributions of reflectance depending on the number of elementary cells (for $N = 5$, 10, 15, and 20) for TM polarization in the 0.3–2.5 μm range. The effect of the number of elementary cells building up the structure on the reflectance is observed. With increasing number of elementary cells, the reflectance value above 1700 nm becomes higher and the transition from low to high reflectance region becomes steeper, although above $N = 15$ the change is barely noticeable which suggests a plateau and the optimum number of ITO/SiO_2 cells to be 15. It is also evident that the transition wavelength does not change significantly with the angle of incidence. The described results of spatial reflectance distributions in Fig. 4 confirm the calculated reflectance values in the studied range illustrated in Fig. 3 (reflectance curves marked in blue).

The following Figure 5 illustrates the spatial distributions of transmittance as a function of incident angle for the same structures constructed from ITO/SiO_2 layers for $N = 5$, 10, 15, and 20. From the analysis of Fig. 5, it can be seen that the spatial distributions of transmittance as a function of incident angle for structures built from ITO/SiO_2 layers also differ with respect to each other. In this case, also the effect of the number of elementary cells on the transmittance is observed. With an increasing number of elementary cells, the transmittance value below 1700 nm becomes lower, while the transition from high to low

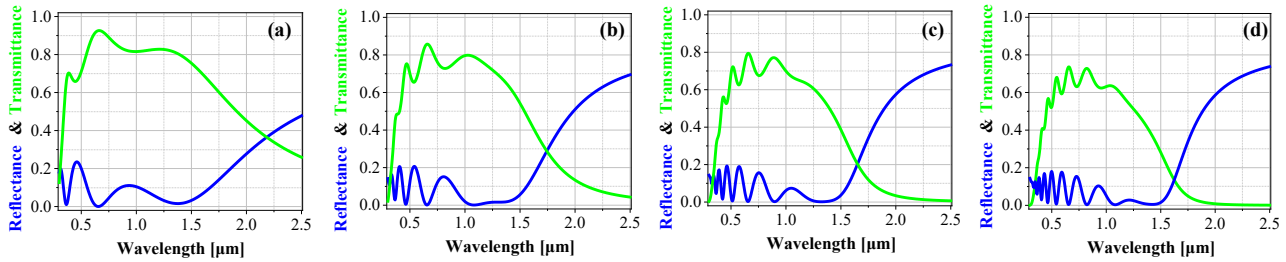

Fig. 3. Simulation results of transmittance and reflectance spectra obtained at an incident angle of 0° for multi-layered structures (20 nm ITO/20 nm SiO_2) for different numbers of elemental cells in the structure, respectively: (a) $N = 5$, (b) $N = 10$, (c) $N = 15$, (d) $N = 20$. Blue colour indicates the reflectance and green the transmittance as a function of wavelength in the range from 0.3 µm to 2.5 µm.

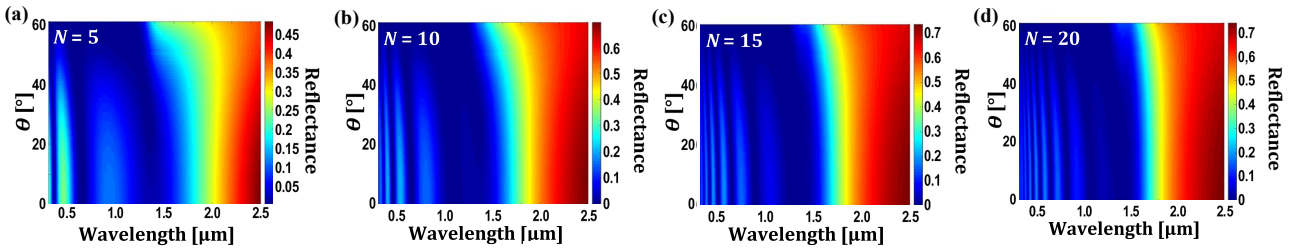

Fig. 4. Spatial distributions of reflectance in the range rom 0.3 µm to 2.5 µm for different angles of incidence of electromagnetic wave in the range from 0° to 60° obtained for multi-layer structures (20 nm ITO/20 nm SiO_2) for different number of elementary cells N in ITO/SiO_2 structure, for TM polarization: (a) for $N = 5$, (b) for $N = 10$, (c) for $N = 15$, (d) for $N = 20$.

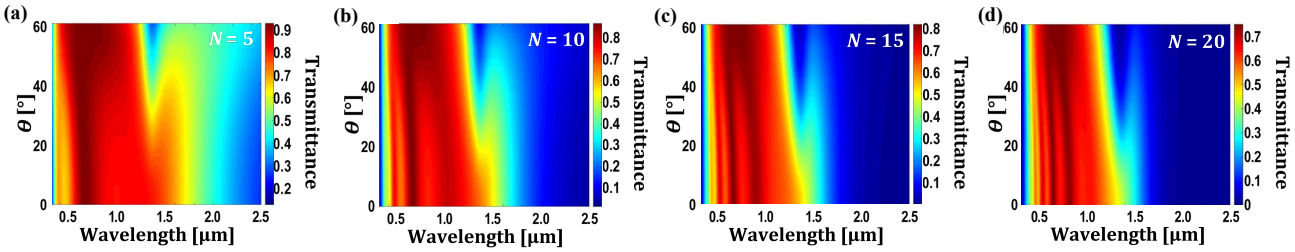

Fig. 5. Spatial distributions of transmittance in the range from 0.3 µm to 2.5 µm for different angles of incidence of electromagnetic wave in the range from 0° to 60° obtained for multi-layer structures (20 nm ITO/20 nm SiO_2) for different number of elementary cells N in ITO/SiO_2 structure, for TM polarization: (a) for $N = 5$, (b) for $N = 10$, (c) for $N = 15$, (d) for $N = 20$.

transmittance becomes steeper, as it was also for reflectance presented in Fig. 4. In the case of transmittance, it is also possible to determine the optimum number of ITO/SiO_2 cells to be 15 which allows maintaining steep transmittance/reflectance transition and relatively high transmittance values. With increasing angle of incidence, starting from about 20°, a dip in the transmission is visible near the wavelength of 1400 nm, effectively limiting the high transmittance range to about 1200 nm. The spatial distributions of transmittance illustrated in Fig. 5 also confirm the calculated transmittance results in the considered range which were previously illustrated in Fig. 3 (curves marked in green).

4. Conclusions

The obtained results of the spatial distributions of transmittance and reflectance using the FDTD method are in full agreement and confirm the trends of other obtained results of the reflectance and transmittance spectra obtained using the TMM method for the studied multi-layer structures of HMMs constructed from ITO/SiO_2 layers. Also, the obtained results confirmed the existence of hyperbolic dispersion of both types of HMMs – Type I and Type II – meaning the structure behaves as an effective dielectric or effective metal, respectively, depending on the wavelength range. Additionally, the analysed HMM structure displayed the possibility of tunability with changes of the number of elementary cells. Hence, the results showed that the designed structures can be used as tunable edge filters in the NIR region. Such filters enable the selective transmission of a part of the spectrum in the form of optical information and generate new perspectives for developing innovative integrated low- and high-pass filters for applications in integrated optical systems.

The implementation of data characterising the material properties of the ITO layers is of great importance. The materials in the TCOs group are, in many cases, composed of mixed oxides, and therefore, the properties of the thin film depend not only on its thickness but also on the fractional content of each of the individual components. The material properties of ITOs are determined by the compound ratio of indium to tin atoms. However, above all – even the determination of these parameters is not yet sufficient, since the properties of the resulting structure (e.g., its homogeneity or surface roughness) also depend on

the technological manufacturing process. That is the reason why directly measured ITO permittivity values were used in simulations to obtain the most realistic properties of HMM structures.

At this point, it is also worth mentioning that ITO can be used as a functional material constituting a layer in a multi-layer structure performing a specific function – either a conductive layer (like metal) or a dielectric layer – depending on the thickness of the layers and the degree of concentration of the tin oxide (SnO_2) fraction relative to indium oxide (In_2O_3) in the layer. A comparison of the properties of TCOs materials such as ITO is presented, among others, in Refs. 23 and 24.

Acknowledgements

This work was supported by the Project UGB/22-723/2024 entitled: “Materials, metamaterials and structures for photonic applications”.

References

[1] Sun, J. & Litchinitser, N. M. Metamaterials. in *Fundamentals and Applications of Nanophotonics* (ed. Haus, J. W.) 253–307 (Elsevier, 2016). https://doi.org/10.1016/B978-1-78242-464-2.00009-9

[2] Shekhar, P., Atkinson, J. & Jacob, Z. Hyperbolic metamaterials: fundamentals and applications. *Nano Converg.* **1**, 14 (2014). https://doi.org/10.1186/s40580-014-0014-6

[3] Tsai, K. T. *et al*. Looking into meta-atoms of plasmonic nanowire metamaterial. *Nano Lett*. **14**, 4971–4976 (2014). https://doi.org/10.1021/nl501283c

[4] Veselago, V. G. The electrodynamics of substances with simultaneously negative values of ε and μ. *Phys.-Uspekhi* **10**, 509–514 (1968). https://doi.org/10.1070/PU1968v010n04ABEH003699

[5] Smith, D. R., Padilla, W., Vier, D. C., Nemat-Nasser, S. & Schultz, S. Composite medium with simultaneously negative permeability and permittivity. *Phys. Rev. Lett*. **84**, 4184–4187 (2000). https://doi.org/10.1103/PhysRevLett.84.4184

[6] Caloz, C. & Itoh, T. *Electromagnetic Metamaterials: Transmission Line Theory and Microwave Applications. The Engineering Approach*. (John Wiley & Sons, 2006). https://doi.org/10.1002/0471754323

[7] Podolskiy, V. A. & Narimanov, E. E. Strongly anisotropic waveguide as a nonmagnetic left-handed system. *Phys. Rev. B* **71**, 201101(R) (2005). https://doi.org/10.1103/PhysRevB.71.201101

[8] Jacob, Z., Alekseyev, L. V. & Narimanov, E. Optical hyperlens: Far-field imaging beyond the diffraction limit. *Opt. Express* **14**, 8247–8256 (2006). https://doi.org/10.1364/OE.14.008247

[9] Smolyaninov, I. I. *Hyperbolic Metamaterials*. (Morgan & Claypool Publishers, 2018). https://doi.org/10.1088/978-1-6817-4565-7

[10] Ferrari, L., Wu, C., Lepage, D., Zhang, X. & Liu, Z. Hyperbolic matermaterials and their applications. *Prog. Quantum Electron*. **40**, 1–40 (2015). https://doi.org/10.1016/j.pquantelec.2014.10.001

[11] Noginow, M. A. *et al*. Controlling spontaneous emission with metamaterials. *Opt. Lett*. **35**, 1863–1865 (2010). https://doi.org/10.1364/OL.35.001863

[12] Jacob, Z. *et al*. Engineering photonic density of states using metamaterials. *Appl. Phys. B* **100**, 215–218 (2010). https://doi.org/10.1007/s00340-010-4096-5

[13] Jacob, Z., Smolyaninov, I. I. & Narimanov, E. E. Broadband Purcell effect: Radiative decay engineering with metamterials. *Appl. Phys. Lett.* **100**, 181105 (2012). https://doi.org/10.1063/1.4710548

[14] Gao, Y., Cortes, C. L., Molesky, S. & Jacob, Z., Brooadband super-Planckian thermal emission from hyperbolic metamaterials. *Appl. Phys. Lett.* **101**, 131106 (2012). https://doi.org/10.1063/1.4754616

[15] Gao, Y. & Jacob, Z. Thermal hyperbolic metamaterials. *Opt. Express* **21**, 15014–15019 (2013). https://doi.org/10.1364/OE.21.015014

[16] Zhukovsky, S. V., Orlov, A. A., Babicheva, V. E., Lavrinenko, A. V. & Sipe, J. E. Photonic-band-gap engineering for volume plasmon polaritons in multiscale multilayer hyperbolic metamaterials. *Phys. Rev. A.* **90**, 013801 (2014). https://doi.org/10.1103/PhysRevA.90.013801

[17] Wu, F., Chen, M. & Xiao, S. Wide-angle polarization selectivity based on anomalous defect mode in photonic crystal containing hyperbolic metamaterials. *Opt. Lett.* **47**, 2153–2156 (2022). https://doi.org/10.1364/OL.455910

[18] Wu, F., Wu, X., Xiao, S., Liu, G. & Li, H. Broadband wide-angle multilayer absorber based on a broadband omnidirectional optical Tamm state. *Opt. Express* **29**, 23976–23987 (2021). https://doi.org/10.1364/OE.434181

[19] Korzeb, K., Gajc, M. & Pawlak, D. A. Compendium of natural hyperbolic metamaterials. *Opt. Express* **1**, 25406–25424 (2015). https://doi.org/10.1364/OE.23.025406

[20] Korobkin, D. *et al*. Measurements of the negative refractive index of sub-diffraction waves propagating in an indefinite permittivity medium. *Opt. Express* **18**, 22734–22746 (2010). https://doi.org/10.1364/OE.18.022734

[21] Pianelli, A. *et al*. Graphene-based hypberbolic metamaterial as a switchable reflection modulator. *Opt. Express* **28**, 6708–6718 (2020). https://doi.org/10.1364/OE.387065

[22] Dudek, M., Kowerdziej, R., Pianelli, A. & Parka, J. Graphene-based tunable microcavity. *Sci. Rep.* **11**, 74 (2021). https://doi.org/10.1038/s41598-020-80022-9

[23] Pianelli, A. *et al*. Active control of dielectric singularities in indium-tin-oxides hyperbolic metamaterials. *Sci. Rep.* **12**, 16961 (2022). https://doi.org/10.1038/s41598-022-21252-x

[24] Naik, G. V., Shalaev, V. M. & Boltasseva, A. Alternative plasmonic materials: Beyond gold and silver. *Adv. Mater.* **25**, 3264–3294 (2013). https://doi.org/10.1002/adma.201205076

[25] Pianelli, A. *et al*. 2D hybrid epsilon near-zero platform for nanophotonics. *Proc. SPIE* **12130**, 121300J (2022). https://doi.org/10.1117/12.2624246

[26] Xu, T. & Lezec, H. J. Visible-frequency asymmetric transmission devices incorporating a hyperbolic metamaterial. *Nat. Commun.* **5**, 4141 (2014). https://doi.org/10.1038/ncomms5141

[27] Ghoshroy, A., Adams, W., Zhang, X. & Güney, D. Ö. Hyperbolic metamaterial as a tunable near-field spatial filter to implement active plasmon-injection loss compensation. *Phys. Rev. Appl.* **10**, 024018 (2018). https://doi.org/10.1103/PhysRevApplied.10.024018

[28] Li, Z. & Gu, Q. Topological hyperbolic metamaterials. *Nanophotonics* **13**, 825–839 (2024). https://doi.org/10.1515/nanoph-2023-0768

[29] Palik, E. D. *Handbook of Optical Constants of Solids* (Academic Press, 1985).